

# Infrared-Assisted Single-Stage Framework for Joint Restoration and Fusion of Visible and Infrared Images under Hazy Conditions

Huafeng Li<sup>1</sup>, Jiaqi Fang<sup>1</sup>, Yafei Zhang<sup>1</sup>, and Yu Liu<sup>2</sup>

<sup>1</sup>Kunming University of Science and Technology

<sup>2</sup>Hefei University of Technology

lhfchina99@kust.edu.cn fangjiaqi@stu.kust.edu.cn zyfeimail@163.com yuliu@hfut.edu.cn

## Abstract

Infrared and visible (IR-VIS) image fusion has gained significant attention for its broad application value. However, existing methods often neglect the complementary role of infrared image in restoring visible image features under hazy conditions. To address this, we propose a joint learning framework that utilizes infrared image for the restoration and fusion of hazy IR-VIS images. To mitigate the adverse effects of feature diversity between IR-VIS images, we introduce a prompt generation mechanism that regulates modality-specific feature incompatibility. This creates a prompt selection matrix from non-shared image information, followed by prompt embeddings generated from a prompt pool. These embeddings help generate candidate features for dehazing. We further design an infrared-assisted feature restoration mechanism that selects candidate features based on haze density, enabling simultaneous restoration and fusion within a single-stage framework. To enhance fusion quality, we construct a multi-stage prompt embedding fusion module that leverages feature supplementation from the prompt generation module. Our method effectively fuses IR-VIS images while removing haze, yielding clear, haze-free fusion results. In contrast to two-stage methods that dehaze and then fuse, our approach enables collaborative training in a single-stage framework, making the model relatively lightweight and suitable for practical deployment. Experimental results validate its effectiveness and demonstrate advantages over existing methods.

## 1. Introduction

Infrared and visible (IR-VIS) image fusion effectively combines the unique information from both infrared and visible images, creating a composite image that integrates their complementary features. This fused image not only provides a comprehensive and accurate scene representation

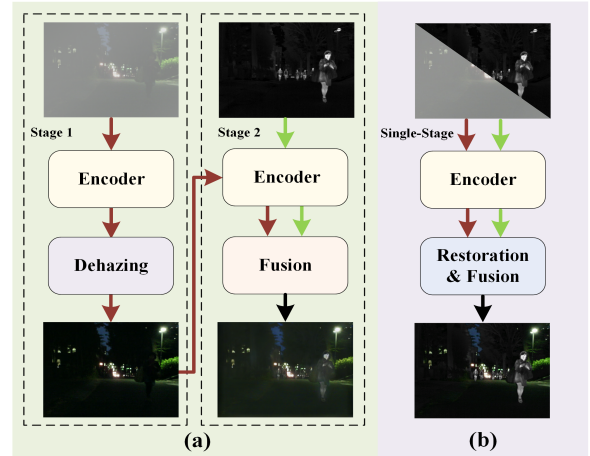


Figure 1. Comparison of existing method and our method for hazy IR-VIS image fusion. (a) The existing method, (b) Our method.

but also significantly aids observers in understanding and analyzing complex environments. Consequently, this technology holds tremendous potential and value in fields such as military reconnaissance, aerospace, environmental monitoring, and medical diagnostics.

In recent years, significant progress has been made in IR-VIS image fusion; however, existing methods generally assume that the input visible images are of good visual quality. In hazy conditions, visible images are affected by haze, resulting in unclear imagery, which makes it difficult for these methods to generate clear, haze-free fusion results. Traditional approaches typically address this issue by first applying a dehazing algorithm to the hazy image and then fusing the dehazed image with the infrared image, as shown in Figure 1(a). Although this two-stage strategy is feasible, it fails to integrate the dehazing and fusion tasks into a unified framework for joint training, making it challenging to balance the relationship between the two tasks. While dehazed images may show good dehazing performance, they are not always optimal for subsequent fusion tasks. Addi-

tionally, the two-stage process of dehazing followed by fusion involves different methodologies, reducing the model’s compactness.

To address the issues arising from the two-stage processing paradigm, Li et al. [20] proposed the all-weather multi-modality image fusion method, which achieves image restoration and fusion under various complex weather conditions. However, this method fails to effectively coordinate the differences between the different restoration tasks, limiting further improvements in restoration and fusion performance. In response, Yi et al. [40] introduced a method called Text-IF, which guides the fusion of degraded images using semantic text. Nevertheless, this approach relies on pre-input text descriptions, increasing the complexity of model deployment. Furthermore, while Text-IF is designed for the restoration and fusion of multiple types of degraded images, it faces challenges in balancing fusion performance across various degradation scenarios without compromising individual task performance.

In response to the challenge of IR-VIS image fusion and restoration under hazy conditions, we propose an infrared-assisted joint learning framework, as shown in Figure 1(b). To mitigate the impact of discrepancies between IR-VIS images on hazy image feature restoration, we design a prompt generation mechanism. It leverages non-shared information from input images to create a prompt selection matrix that selects and generates prompt embeddings from a prompt pool. These embeddings act as candidate features to aid in the recovery of hazy image features. For effective restoration of haze-affected features, we construct an infrared-assisted feature restoration module. It guides the selection of candidate features based on haze density to restore visible image features impacted by haze, enabling the joint processing of restoration and fusion within a single-stage framework. In this process, our focus shifts from solely enhancing the restoration of hazy visible images to emphasizing how restored features can further improve the quality of the fusion results.

To further enhance the fusion effect, we propose a multi-stage prompt embedding fusion module, which strengthens feature restoration and fusion with the help of the feature supplementation capability of the prompt generation. The proposed method not only effectively fuses IR-VIS images but also eliminates the interference of haze, producing clear and haze-free fusion results. Compared to the traditional two-stage approach of first dehazing and then fusing, our method more fully exploits the correlation between dehazing and fusion tasks, achieving a balance between them through a single-stage framework with collaborative training. Furthermore, the model structure is relatively lightweight and compact, facilitating practical deployment. Unlike existing multi-task fusion frameworks, our method is specifically designed for IR-VIS image fusion

and restoration under hazy conditions, demonstrating excellent fusion and restoration performance. Therefore, our approach enriches the technical system for IR-VIS image fusion under hazy conditions and provides a new perspective for the restoration and fusion of low-quality images. In summary, the main contributions and advantages of our method are reflected in the following aspects:

- **Innovative Joint Framework.** An infrared-assisted joint learning framework for IR-VIS image fusion in hazy conditions is proposed, enabling collaborative training of dehazing and fusion tasks in a single stage. Compared to traditional two-stage methods, this framework more efficiently leverages the correlation between dehazing and fusion tasks, allowing them to complement each other and achieve a balanced outcome.
- **Prompt Generation Module and Multi-Stage Fusion.** A prompt generation module is designed to create a prompt selection matrix leveraging non-shared information to intelligently select and embed prompts that assist visible image restoration under hazy conditions. This approach not only enhances the restoration of visible image features but also minimizes the adverse impact of modality differences between IR-VIS features. Furthermore, a multi-stage feature fusion mechanism based on prompt embeddings is proposed to facilitate feature compensation and refinement, further improving the fusion result.
- **Efficient and Compact Model Structure.** The proposed method adopts a single-stage processing framework, making it more compact than the traditional two-stage dehazing and fusion approach, thereby facilitating a better balance between the two tasks. Furthermore, the method efficiently coordinates the dehazing and fusion, enabling the restored image features to more effectively support the generation of clear, haze-free, high-quality fusion results. This design not only enhances the fusion effect but also improves the model’s applicability.

## 2. Related Work

### 2.1. Typical Fusion Methods

In IR-VIS image fusion, traditional methods based on multi-scale transforms and sparse representations [11, 12, 14, 22, 46] remain relevant. However, deep learning-based techniques have become mainstream. These methods can be categorized into three types: Convolutional Neural Network (CNN)-based methods [15, 16, 23], hybrid CNN-Transformer methods [3, 5, 17, 33], and Generative Adversarial Network (GAN)-based methods [18, 21, 25, 26, 35, 39, 47]. CNN-based methods extract features from input images and perform fusion using specialized modules, enhancing image details and contrast. However, CNNs are limited in modeling long-range dependencies, which impacts fusion quality in complex scenes. In contrast, Trans-

formers excel at capturing long-range dependencies but struggle with local details and edges. Hybrid methods, such as AFT [3], YDTR [33], and HitFusion [5], combine CNN with Transformer to model local and global information, improving fusion performance.

In GAN-based methods, FusionGAN [25] uses a single discriminator to fuse IR-VIS images, which does not maintain modality balance, leading to biased fusion results. To address this, subsequent research introduced dual discriminator-based GAN methods. For example, LGM-GAN [35] combines a Conditional GAN with dual discriminators to fuse multi-modality information effectively. DDC-GAN [26] uses dual discriminators for multi-resolution fusion, improving consistency across scales. Moreover, AttentionFGAN [18] integrates an attention mechanism to focus on important feature regions, significantly enhancing fusion performance. However, these methods assume that the images to be fused are of high quality, which makes it challenging to produce high-quality fusion results under hazy conditions.

## 2.2. Methods Under Complex Imaging Conditions

Under complex imaging conditions, various factors affect the quality of visible images. Thus, achieving high-quality fusion results under these conditions has become a crucial research direction in the field of IR-VIS image fusion. In low-light conditions, PIAFusion [31] improves IR-VIS image fusion by introducing an illumination-aware loss function. DIVFusion [32] enhances dark areas, details, and reduces color distortion by separating scene illumination and enhancing texture contrast, achieving high-quality fusion in nighttime conditions. IAIFNet [38] uses an illumination enhancement network along with adaptive difference fusion and salient object awareness modules to better fuse features in IR-VIS images. LENFusion [6] generates high-contrast fusion results through three stages: brightness adjustment, enhancement, and feedback. For low-resolution images, HKD-FS [34] employs knowledge distillation to convert low-resolution IR-VIS images into high-resolution outputs. MLFusion [13] incorporates meta-learning into the IR-VIS image fusion framework, enabling fusion from inputs of any resolution to outputs of any resolution.

To address the degradation of visible images under complex conditions, a decomposition-based, interference-aware fusion method was proposed [19], which effectively fuses degraded IR-VIS images, including noisy, overexposed, and snowy images, but does not address hazy conditions. To address this, AWFusion [20] introduces a clear feature prediction module based on the atmospheric scattering model, enabling dehazing capabilities. However, AWFusion also considers other weather conditions like snow and rain, which reduces its effectiveness in hazy conditions. To balance these tasks, Text-IF [40] uses text guidance for fusion by

generating modulation parameters to control cross-attention outputs, but it is not specifically designed for hazy IR-VIS fusion, resulting in suboptimal performance. Additionally, the need for text input limits its convenience. VIFNet [41] restores hazy images using infrared images, but it focuses only on dehazing and does not address fusion. In contrast, this paper specifically focuses on IR-VIS fusion in hazy conditions to achieve clear, haze-free results.

## 3. Methodology

### 3.1. Overview

As shown in Figure 2, our method comprises three core modules: the Infrared-Assisted Feature Restoration Module (IA-FRM), the Prompt Generation Module (PGM), and the Multi-stage Prompt Embedding Fusion Module (MsPE-FM). IA-FRM leverages infrared image features to assist in restoring lost information in heavily hazy regions of visible images, making it easier to restore these hazy areas. PGM generates a set of prompts to overcome the limitations of infrared images when assisting in the restoration of features in these dense hazy regions. Using the restored visible image features and prompts from PGM, MsPE-FM performs the fusion of IR-VIS image features, reconstructing a haze-free fused result.

### 3.2. Prompt generation

Infrared imaging sensors maintain performance in hazy conditions, allowing them to penetrate heavy haze. In a rigorously registered pair of IR-VIS images  $I_{ir}, I_{vi}$  provided to the model, we assume that only the visible image  $I_{vi}$  contains haze, while the infrared image  $I_{ir}$  is unaffected by haze. The core challenge of this work is to effectively utilize the infrared image  $I_{ir}$  to restore the visible image  $I_{vi}$  and then fuse them. However, the significant modality differences between IR-VIS images make it difficult to rely solely on the infrared image  $I_{ir}$  to recover the details lost in the hazy visible image. To overcome these challenges, this paper proposes the PGM, which generates a prompt embedding to create compensatory features that address the limitations of infrared features.

As shown in Figure 2, in the PGM, we first utilize an encoder constructed with Restormer [43] to perform feature encoding on the input registered IR-VIS images  $\{I_{ir}, I_{vi}\}$ . As depicted in Figure 2(a), Restormer consists of a self-attention layer and a feed-forward network layer. The features output by the Restormer encoder are denoted as  $F_{vi} \in \mathbb{R}^{C \times H \times W}$  and  $F_{ir} \in \mathbb{R}^{C \times H \times W}$ , where  $C$ ,  $H$ , and  $W$  represent the number of channels, height, and width of the features, respectively. Additionally, in this module, the features of the hazy visible image  $I_{vi}$  and the infrared image  $I_{ir}$  are processed by:

$$F_{vi-ir} = F_{vi} - F_{ir} \quad (1)$$

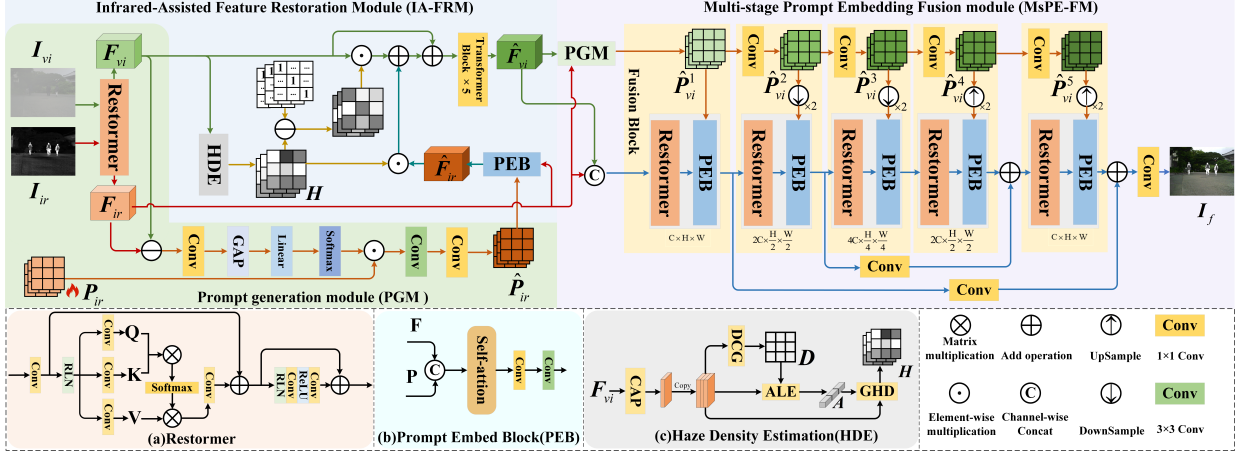


Figure 2. Overall framework of the proposed method. The input IR and hazy VIS image pair  $\{I_{ir}, I_{vi}\}$  is processed by the PGM to obtain features  $\{F_{ir}, F_{vi}\}$  and a prompt  $P_{ir}$  for  $F_{ir}$ . Through the PEB, the prompt embedding  $\hat{P}_{ir}$  is used to refine the IR feature  $F_{ir}$ , reducing redundant information and generating the refined IR feature  $\hat{F}_{ir}$ . The HDE module [9] estimates the haze density in the VIS features to dynamically adjust the proportion of injected IR information, preventing excessive IR injection. The Transformer block removes degradation from the input features to obtain haze-free features. In the MsPE-FM, the haze-free VIS features and IR features are combined and passed to the Fusion Block for feature fusion. The PGM and PEB further are used to enhance the IR-VIS complementary information, reconstructing the final fused image.

to remove the shared information and highlight the unique information. The resulting difference  $F_{vi-ir}$  is then fed into a weight prediction network composed of Convolutional (Conv) layer, GAP, Linear layer, and Softmax, resulting in a weight matrix  $W_p \in \mathbb{R}^{C \times H \times W}$  for selecting prompt information from the prompt pool  $P_{ir}$ . At this stage, the prompt embedding generated for compensating the infrared image features can be represented as:

$$\hat{P}_{ir} = \text{Conv}_{3 \times 3} (\text{Conv}_{1 \times 1} (W_p \odot P_{ir})) \quad (2)$$

where  $P_{ir} \in \mathbb{R}^{C \times H \times W}$  is a learnable prompt pool,  $\text{Conv}_{3 \times 3}$  and  $\text{Conv}_{1 \times 1}$  denote  $3 \times 3$  and  $1 \times 1$  Conv layers, respectively. The resulting  $\hat{P}_{ir}$  is then fed, along with the infrared image features  $F_{ir}$ , into the Prompt Embedding Block (PEB) to obtain the features  $\hat{F}_{ir}$  for compensating the dense haze regions in the visible image  $I_{vi}$ .

### 3.3. Feature restoration assisted by infrared image

To effectively utilize the information provided by the infrared image  $I_{ir}$  for restoring features in haze regions, we design the IA-FRM. As shown in Figure 2, when restoring features in hazy images, regions with higher haze density should receive more focus. Therefore, it is essential to estimate the haze density in the input images. To achieve this, we adopt the method from [9] to estimate the haze density in the input image features, as illustrated in Figure 2(c). Specifically, the dark channel information of  $F_{vi}$  is obtained through the Dark Channel Generation (DCG) operation. The resulting dark channel information, along with the feature  $\hat{F}_{vi}$ , is then fed into the Atmospheric Light Estimation (ALE) module to predict the atmospheric light,

denoted as  $A$ . Here,  $\hat{F}_{vi}$  is obtained by applying Channel Average Pooling (CAP) to  $F_{vi}$ , followed by channel replication. Based on  $A$  and  $\hat{F}_{vi}$ , we can obtain the initial transmission map for each pixel location through the Get Haze Density (GHD) block, as shown in Eq. (3):

$$T = 1 - \omega \cdot \text{DCG} (\hat{F}_{vi} \odot A^{-1}) \quad (3)$$

where  $\omega$  is a constant that adjusts the effect of the DCG prediction, set to 0.95 as suggested in [9];  $\mathbf{1} \in \mathbb{R}^{1 \times H \times W}$  is a matrix of ones; and  $A^{-1}$  represents the element-wise reciprocal of the atmospheric light  $A$ , which is broadcast along the channel dimension to match the dimension of  $\hat{F}_{vi}$ .

Then, in the GHD block, the transmission map  $T$  is refined using a guided filter, yielding the refined transmission map  $T'$ . Since the transmission map is inversely proportional to the haze density, we estimate the haze density  $H$  through the following equation:

$$H = 1 - T' \quad (4)$$

In  $H$ , the higher the haze density, the larger the corresponding value. Therefore,  $H$  is used to select the information for restoring  $F_{vi}$  from  $\hat{F}_{ir}$ . In this process, we use  $(1 - H)$  to remove the information from regions with heavier haze in  $F_{vi}$  and replace it with corresponding information from  $\hat{F}_{ir}$  to assist in restoring these regions. The specific process can be formulated as:

$$\hat{F}_{vi} = TF (\hat{F}_{ir} \odot H + F_{vi} \odot (1 - H) + F_{vi}) \quad (5)$$

where  $TF$  denotes Transformer block. To ensure the quality of  $\hat{F}_{vi}$ , it is passed through a  $3 \times 3$  Conv to obtain the



dehazed image  $\hat{\mathbf{I}}_{vi}$ , and  $L_1$ -loss is used to optimize the network:

$$\ell_1 = \left\| \hat{\mathbf{I}}_{vi} - \mathbf{I}_{vi,gt} \right\|_1 \quad (6)$$

Here,  $\mathbf{I}_{vi,gt}$  represents the corresponding ground truth haze-free visible image.

### 3.4. Multi-stage Prompt Embedding Fusion

With the assistance of infrared features  $\hat{\mathbf{F}}_{ir}$ , we obtain the dehazed visible image features  $\hat{\mathbf{F}}_{vi}$ . These features are then fused with the infrared image features  $\mathbf{F}_{ir}$  to reconstruct a dehazed fusion result. This approach enables us to fuse hazy IR-VIS images within a single framework, producing a dehazed fusion output. In this process, an effective fusion method is essential to achieve high-quality fusion results. To prevent residual haze in  $\hat{\mathbf{F}}_{vi}$  from affecting the fusion, we propose the MsPE-FM.

As shown in Figure 2, in the MsPE-FM, the restored feature  $\hat{\mathbf{F}}_{vi}$  and the initial feature  $\mathbf{F}_{ir}$  are input into the PGM to obtain the prompt embedding  $\hat{\mathbf{P}}_{vi}^1$  at the first stage of the fusion process. After concatenating  $\hat{\mathbf{F}}_{vi}$  and  $\mathbf{F}_{ir}$ , the result is passed through the Restormer [43]. This output, along with  $\hat{\mathbf{P}}_{vi}^1$ , is then input into the PEB to obtain the fusion result for the next stage. In the second stage,  $\hat{\mathbf{P}}_{vi}^1$  is first passed through a  $1 \times 1$  Conv layer to adjust the number of channels, resulting in the adjusted prompt embedding  $\hat{\mathbf{P}}_{vi}^2$ , which adapts to the changes in feature channels during the second-stage feature extraction. In this fusion process, five fusion blocks, each consisting of prompt embeddings, a Restormer, and a PEB, are used to achieve the fusion of IR-VIS features. Within these fusion blocks, two residual connections are employed to prevent information loss. Finally, the fused features pass through a  $1 \times 1$  Conv layer to reconstruct the fused result  $\mathbf{I}_f$ .

To ensure that the gradients of the fusion result are consistent with those of the input infrared image and the clear visible image across the three RGB channels, we employ the gradient loss from [42] to optimize the parameters of the entire network:

$$\ell_{\nabla} = \frac{1}{HW} \sum_{i=1}^3 \left\| \nabla \mathbf{I}_f^i - \max(|\nabla \mathbf{I}_{ir}^i|, |\nabla \mathbf{I}_{vi,gt}^i|) \right\|_1 \quad (7)$$

where  $\nabla$  denotes the gradient operator, and  $i$  represents the R, G, B channels. Additionally, to ensure that the fused image maintains consistent pixel intensity with both the IR and VIS images, we utilize a pixel intensity consistency loss function  $\ell_{int}$  to update the network parameters:

$$\ell_{int} = \frac{1}{HW} \sum_{i=1}^3 \left\| \mathbf{I}_f^i - \max(\mathbf{I}_{ir}^i, \mathbf{I}_{vi,gt}^i) \right\|_1 \quad (8)$$

The total loss is then formulated as:

$$\ell_{total} = \ell_{int} + \ell_{\nabla} + \alpha \ell_1 \quad (9)$$

where  $\alpha$  is a hyperparameter that adjusts the contribution of the  $L_1$ -loss in this optimization process.

## 4. Experiments

### 4.1. Experiment Settings

**Datasets and Training Details.** In this work, we utilize 1,083 IR-VIS image pairs from the MSRS dataset [31] as the training set. For the test set, we select 361 pairs from MSRS (ensuring no overlap with the training set), 50 pairs from RoadScene [36], and 100 pairs from M<sup>3</sup>FD [21]. To generate hazy image pairs, we apply the atmospheric scattering model [27] to introduce haze into the visible images in both the training and test sets. All experiments are conducted using the PyTorch framework on a single 24GB NVIDIA GeForce RTX 4090 GPU. During training, images are randomly cropped to  $256 \times 256$  patches, with data augmentation techniques such as horizontal and vertical flipping applied. The model is trained for a total of 300 epochs, using a batch size of 6 and the AdamW optimizer [10]. The initial learning rate is set to  $2 \times 10^{-4}$  and is gradually reduced to  $2 \times 10^{-6}$  following a cosine annealing schedule.

**Metrics.** To objectively evaluate the fusion performance of different methods, we adopt five commonly used image quality assessment metrics: Mutual Information ( $Q_{MI}$ ) [29], Gradient-based Fusion Performance ( $Q_{AB/F}$ ) [37], Chen-Varshney Metric ( $Q_{CV}$ ) [4], Sum of Correlation of Differences ( $Q_{SCD}$ ) [1], and Visual Information Fidelity ( $Q_{VIF}$ ) [8]. These metrics assess the quality of the fusion results, using clear source images (without haze) as reference images when necessary. Additionally, to evaluate the perceptual quality of the dehazing effects within the fusion results, we employ the Perceptual Index ( $Q_{PI}$ ) [2], Natural Image Quality Evaluator ( $Q_{NIQE}$ ) [28], and Spatial Frequency ( $Q_{SF}$ ) [7]. According to the evaluation criteria, lower  $Q_{CV}$ ,  $Q_{PI}$ , and  $Q_{NIQE}$  values indicate better fusion performance, while higher values for the remaining metrics signify improved quality.

### 4.2. Comparison with State-of-the-art Methods

There are two existing methodologies for fusing hazy visible images with infrared images. The first methodology involves initially applying advanced image dehazing algorithms to remove haze from the visible images, followed by fusing the dehazed images with the infrared images. For this purpose, we select the latest and most effective dehazing methods, specifically DIACMP [45] and Dehazformer [30]. Next, we apply representative IR-VIS image fusion methods, such as MLFusion [13], U2Fusion [36], LRRNet [15], ALFusion [17], TIMFusion [24], and MRFS [44], to fuse the dehazed visible images with the infrared images. The second methodology employs the Text-IF method [40], which directly restores and fuses hazy images with the as-



Figure 3. Visual comparison of fusion results from different methods. In the fusion results produced by the comparison methods, the first row of each image pair (except for the last column) shows the result after dehazing with DIACMP, followed by fusion. The second row shows the result after dehazing with Dehazeformer, followed by fusion. The last column presents the fusion results of Text-IF and our method.

sistance of text information.

Figure 3 sequentially displays the visual effects of fusion results obtained using different methods on the MSRS, M<sup>3</sup>FD, and RoadScene datasets. As shown in Figure 3, our method not only effectively removes haze but also successfully integrates complementary information from the IR-VIS images, producing clear and coherent fusion results. Furthermore, our approach efficiently restores brightness

information, enhancing overall contrast while avoiding the introduction of noise into the image. In contrast, alternative methods, which treat dehazing and fusion as independent processes, do not facilitate effective fusion during the dehazing stage, resulting in lower-quality fusion outcomes. When faced with complex weather conditions, traditional dehazing methods often struggle to accurately restore sky regions. However, our proposed end-to-end joint frame-



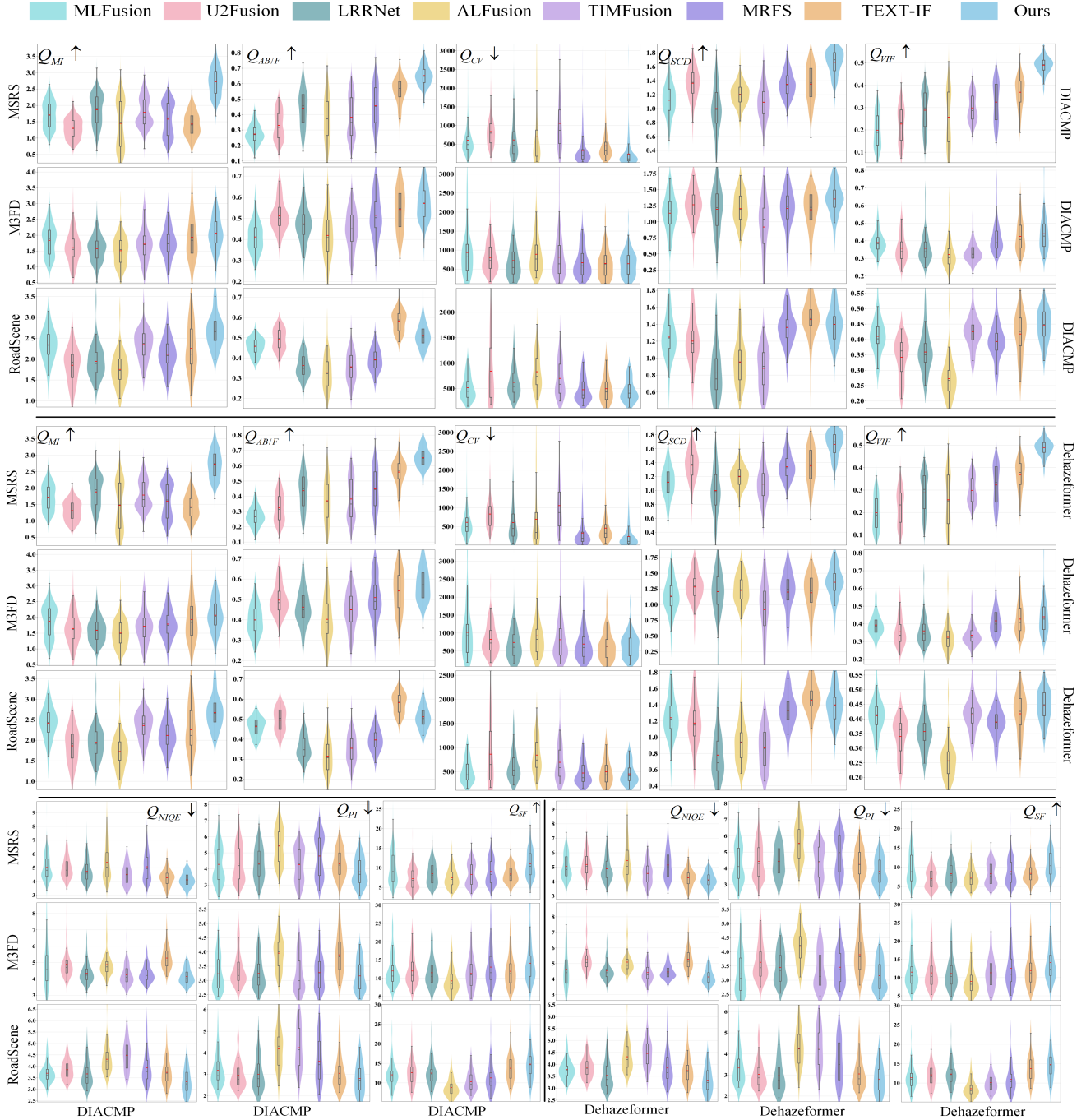


Figure 4. Visualization of objective evaluation results. The comparison is divided into three groups: the first group shows the results of using DIACMP for dehazing followed by fusion on MSRS, M3FD, and RoadScene; the second group shows the results of using Dehazformer for dehazing followed by fusion on the same datasets; the third group presents the objective evaluation results of fusion images obtained using different dehazing methods, assessed with haze evaluation metrics.

work, leveraging infrared information, effectively helps the network restore these sky regions, thereby achieving superior restoration and fusion results. Additionally, while the Text-IF can perform both dehazing and fusion, it does not exhibit significant advantages in either task.

To further substantiate the advantages of our method,

we present violin plots that quantitatively compare our approach with traditional methods. **The detailed data comparison can be found in the supplementary materials.** As illustrated in the figure 4, our method consistently outperforms others across three different datasets and five evaluation metrics, demonstrating a more concentrated data



Figure 5. Effect of different modules on fusion performance.

Table 1. Quantitative results of six ablation experiments on the MSRS dataset, with the values in red indicating the best performance and those in blue indicating the second-best.

Models	$Q_{PI} \downarrow$	$Q_{NIQE} \downarrow$	$Q_{AB/F} \uparrow$	$Q_{VIF} \uparrow$	$Q_{SCD} \uparrow$	$Q_{CV} \downarrow$	$Q_{MI} \uparrow$	$Q_{SF} \uparrow$
w/o $F_{ir}$	3.866	4.217	0.651	0.483	1.631	252.400	2.520	11.120
w/o HDE	3.887	4.319	0.644	0.464	1.585	253.014	2.337	10.657
w/o $\hat{P}_{ir}$	3.851	4.259	0.648	0.481	1.628	246.616	2.521	10.848
w/o FR-PEB	3.819	4.099	0.644	0.475	1.601	251.357	2.349	10.942
w/o $\hat{P}_{vi}$	3.820	4.212	0.638	0.478	1.598	294.239	2.132	10.902
w/o FB-PEB	3.846	4.115	0.645	0.481	1.656	241.963	2.607	10.854
Ours	3.811	4.110	0.652	0.490	1.662	238.420	2.720	11.050

distribution, which indicates more robust and stable performance in hazy image fusion. Moreover, our method achieves the best average performance among all methods in terms of the  $Q_{PI}$ ,  $Q_{NIQE}$ , and  $Q_{SF}$ , further affirming the exceptional restoration capabilities of our model.

### 4.3. Ablation Study

We design six experimental settings to evaluate the effectiveness of each module. In the first setting, we remove the PGM-generated prompt  $\hat{P}_{ir}$ , the HDE module, and the process of supplementing visible features with infrared features based on haze density, directly inputting  $F_{vi}$  into the Transformer Block for dehazing (denoted as “w/o  $F_{ir}$ ”) to assess the auxiliary role of infrared information. In the second setting, we replace the operation in Eq. (5) by directly adding  $\hat{F}_{ir}$  and  $F_{vi}$  (denoted as “w/o HDE”) to validate the impact of haze-density-based infrared integration. In the third setting, we remove the prompt embedding for  $\hat{P}_{ir}$  and the PEB module, injecting infrared features extracted by the encoder, guided by haze density  $H$ , directly into  $F_{vi}$  (denoted as “w/o  $\hat{P}_{ir}$ ”) to evaluate the effect of prompt embedding. In the fourth setting, we test the effectiveness of the PEB module by removing it from IA-FRM, denoted as “w/o FR-PEB”. In the fifth setting, we remove  $\hat{P}_{vi}$  from MsPE-FM to verify the effectiveness of prompt embedding, denoted as “w/o  $\hat{P}_{vi}$ ”. In the sixth setting, we omit the PEB from the Fusion Block, performing feature concatenation and convolution directly (denoted as “w/o FB-PEB”) to validate its role in fusion.

Table 1 and Figure 5 demonstrate the impact of each module on fusion performance. While removing any module leads to performance decrease, these changes may not

be readily visible in the qualitative results but are clearly reflected in the quantitative data. As shown in Table 1, when infrared information is not used to supplement visible features, the metrics  $Q_{PI}$  and  $Q_{NIQE}$  increase significantly, and all fusion metrics decrease, confirming the effectiveness of incorporating infrared information to enhance visible features. If the HDE module is excluded, and infrared information is directly injected into the visible image, model performance does not improve. Instead, color distortion appears in the fusion results, and objective evaluation metrics decline to varying degrees. Similar issues are observed in Setting 3. Additionally, Setting 4 through 6 show slight degradation in detail retention, along with a decline in objective metrics, further validating the effectiveness of each module. **Additional experiments, including hyperparameter analysis, model complexity comparisons, and discussions on method limitations and future work, are provided in the supplementary materials.**

## 5. Conclusion

This paper presents an infrared-assisted joint learning framework for IR-VIS image fusion under hazy conditions. By integrating dehazing and fusion tasks into a single-stage framework with collaborative training, our method effectively enhances feature restoration and fusion performance. Experimental results demonstrate that our approach produces clear, haze-free fusion images, outperforming traditional two-stage methods and existing multi-task fusion frameworks. The lightweight and compact model structure also ensures practical deployment, making it a valuable solution for hazy image restoration and fusion.



## References

- [1] V Aslantas and Emre Bendes. A new image quality metric for image fusion: The sum of the correlations of differences. *Aeu-International Journal of Electronics and Communications*, 69(12):1890–1896, 2015. 5
- [2] Yochai Blau, Roey Mechrez, Radu Timofte, Tomer Michaeli, and Lihi Zelnik-Manor. The 2018 pirm challenge on perceptual image super-resolution. In *Proceedings of the European Conference on Computer Vision Workshops (ECCVW)*, pages 334–355, 2018. 5
- [3] Zhihao Chang, Zhixi Feng, Shuyuan Yang, and Quanwei Gao. Aft: Adaptive fusion transformer for visible and infrared images. *IEEE Transactions on Image Processing*, 32: 2077–2092, 2023. 2, 3
- [4] Hao Chen and Pramod K Varshney. A human perception inspired quality metric for image fusion based on regional information. *Information Fusion*, 8(2):193–207, 2007. 5
- [5] Jun Chen, Jianfeng Ding, and Jiayi Ma. Hitfusion: Infrared and visible image fusion for high-level vision tasks using transformer. *IEEE Transactions on Multimedia*, 26:10145–10159, 2024. 2, 3
- [6] Jun Chen, Liling Yang, Wei Liu, Xin Tian, and Jiayi Ma. Lenfusion: A joint low-light enhancement and fusion network for nighttime infrared and visible image fusion. *IEEE Transactions on Instrumentation and Measurement*, 73:1–15, 2024. 3
- [7] Ahmet M Eskicioglu and Paul S Fisher. Image quality measures and their performance. *IEEE Transactions on Communications*, 43(12):2959–2965, 1995. 5
- [8] Yu Han, Yunze Cai, Yin Cao, and Xiaoming Xu. A new image fusion performance metric based on visual information fidelity. *Information Fusion*, 14(2):127–135, 2013. 5
- [9] Kaiming He, Jian Sun, and Xiaoou Tang. Single image haze removal using dark channel prior. *IEEE Transactions on Pattern Analysis and Machine Intelligence*, 33(12):2341–2353, 2011. 4
- [10] Diederik P. Kingma and Jimmy Ba. Adam: A method for stochastic optimization. In *International Conference on Learning Representations (ICLR)*, 2015. 5
- [11] Hui Li and Xiao-Jun Wu. Densefuse: A fusion approach to infrared and visible images. *IEEE Transactions on Image Processing*, 28(5):2614–2623, 2019. 2
- [12] Huafeng Li, Yitang Wang, Zhao Yang, Ruxin Wang, Xiang Li, and Dapeng Tao. Discriminative dictionary learning based multiple component decomposition for detail-preserving noisy image fusion. *IEEE Transactions on Instrumentation and Measurement*, 69(4):1082–1102, 2020. 2
- [13] Huafeng Li, Yueliang Cen, Yu Liu, Xun Chen, and Zhengtao Yu. Different input resolutions and arbitrary output resolution: A meta learning-based deep framework for infrared and visible image fusion. *IEEE Transactions on Image Processing*, 30:4070–4083, 2021. 3, 5
- [14] Hui Li, Xiao-Jun Wu, and Josef Kittler. Rfn-nest: An end-to-end residual fusion network for infrared and visible images. *Information Fusion*, 73:72–86, 2021. 2
- [15] Hui Li, Tianyang Xu, Xiao-Jun Wu, Jiwen Lu, and Josef Kittler. Lrnnet: A novel representation learning guided fusion network for infrared and visible images. *IEEE Transactions on Pattern Analysis and Machine Intelligence*, 45(9):11040–11052, 2023. 2, 5
- [16] Huafeng Li, Junzhi Zhao, Jinxing Li, Zhengtao Yu, and Guangming Lu. Feature dynamic alignment and refinement for infrared–visible image fusion: Translation robust fusion. *Information Fusion*, 95:26–41, 2023. 2
- [17] Huafeng Li, Junyu Liu, Yafei Zhang, and Yu Liu. A deep learning framework for infrared and visible image fusion without strict registration. *International Journal of Computer Vision*, 132:1625–1644, 2024. 2, 5
- [18] Jing Li, Hongtao Huo, Chang Li, Renhua Wang, and Qi Feng. Attentionfgan: Infrared and visible image fusion using attention-based generative adversarial networks. *IEEE Transactions on Multimedia*, 23:1383–1396, 2021. 2, 3
- [19] Xilai Li, Xiaosong Li, and Haishu Tan. Decomposition based and interference perception for infrared and visible image fusion in complex scenes. *arXiv preprint arXiv: 2402.02096*, 2024. 3
- [20] Xilai Li, Wuyang Liu, Xiaosong Li, and Haishu Tan. Physical perception network and an all-weather multi-modality benchmark for adverse weather image fusion. *arXiv preprint arXiv: 2402.02090*, 2024. 2, 3
- [21] Jinyuan Liu, Xin Fan, Zhanbo Huang, Guanyao Wu, Risheng Liu, Wei Zhong, and Zhongxuan Luo. Target-aware dual adversarial learning and a multi-scenario multi-modality benchmark to fuse infrared and visible for object detection. In *Proceedings of the IEEE/CVF Conference on Computer Vision and Pattern Recognition (CVPR)*, pages 5802–5811, 2022. 2, 5
- [22] Jinyuan Liu, Xin Fan, Ji Jiang, Risheng Liu, and Zhongxuan Luo. Learning a deep multi-scale feature ensemble and an edge-attention guidance for image fusion. *IEEE Transactions on Circuits and Systems for Video Technology*, 32(1): 105–119, 2022. 2
- [23] Jinyuan Liu, Runjia Lin, Guanyao Wu, Risheng Liu, Zhongxuan Luo, and Xin Fan. Coconet: Coupled contrastive learning network with multi-level feature ensemble for multi-modality image fusion. *International Journal of Computer Vision*, 132(5):1748–1775, 2024. 2
- [24] Risheng Liu, Zhu Liu, Jinyuan Liu, Xin Fan, and Zhongxuan Luo. A task-guided, implicitly-searched and metainitialized deep model for image fusion. *IEEE Transactions on Pattern Analysis and Machine Intelligence*, 46(10):6594–6609, 2024. 5
- [25] Jiayi Ma, Wei Yu, Pengwei Liang, Chang Li, and Junjun Jiang. Fusiongan: A generative adversarial network for infrared and visible image fusion. *Information Fusion*, 48:11–26, 2019. 2, 3
- [26] Jiayi Ma, Han Xu, Junjun Jiang, Xiaoguang Mei, and Xiaoping Zhang. Ddcgan: A dual-discriminator conditional generative adversarial network for multi-resolution image fusion. *IEEE Transactions on Image Processing*, 29:4980–4995, 2020. 2, 3
- [27] William Edgar Knowles Middleton. *Vision through the atmosphere*. University of Toronto Press, 1952. 5

- [28] Anish Mittal, Rajiv Soundararajan, and Alan C. Bovik. Making a “completely blind” image quality analyzer. *IEEE Signal Processing Letters*, 20(3):209–212, 2013. 5
- [29] Guihong Qu, Dali Zhang, and Pingfan Yan. Information measure for performance of image fusion. *Electronics Letters*, 38(7):1, 2002. 5
- [30] Yuda Song, Zhuqing He, Hui Qian, and Xin Du. Vision transformers for single image dehazing. *IEEE Transactions on Image Processing*, 32:1927–1941, 2023. 5
- [31] Linfeng Tang, Jiteng Yuan, Hao Zhang, Xingyu Jiang, and Jiayi Ma. Piafusion: A progressive infrared and visible image fusion network based on illumination aware. *Information Fusion*, 83-84:79–92, 2022. 3, 5
- [32] Linfeng Tang, Xinyu Xiang, Hao Zhang, Meiqi Gong, and Jiayi Ma. Divfusion: Darkness-free infrared and visible image fusion. *Information Fusion*, 91:477–493, 2023. 3
- [33] Wei Tang, Fazhi He, and Yu Liu. Ydtr: Infrared and visible image fusion via y-shape dynamic transformer. *IEEE Transactions on Multimedia*, 25:5413–5428, 2022. 2, 3
- [34] Wanxin Xiao, Yafei Zhang, Hongbin Wang, Fan Li, and Hua Jin. Heterogeneous knowledge distillation for simultaneous infrared-visible image fusion and super-resolution. *IEEE Transactions on Instrumentation and Measurement*, 71:1–15, 2022. 3
- [35] Han Xu, Pengwei Liang, Wei Yu, Junjun Jiang, and Jiayi Ma. Learning a generative model for fusing infrared and visible images via conditional generative adversarial network with dual discriminators. In *Proceedings of the Twenty-Eighth International Joint Conference on Artificial Intelligence (IJCAI)*, pages 3954–3960, 2019. 2, 3
- [36] Han Xu, Jiayi Ma, Junjun Jiang, Xiaojie Guo, and Haibin Ling. U2fusion: A unified unsupervised image fusion network. *IEEE Transactions on Pattern Analysis and Machine Intelligence*, 44(1):502–518, 2022. 5
- [37] Costas S Xydeas, Vladimir Petrovic, et al. Objective image fusion performance measure. *Electronics Letters*, 36(4):308–309, 2000. 5
- [38] Qiao Yang, Yu Zhang, Zijing Zhao, Jian Zhang, and Shunli Zhang. Iaifnet: An illumination-aware infrared and visible image fusion network. *IEEE Signal Processing Letters*, 31:1374–1378, 2024. 3
- [39] Yong Yang, Jiaxiang Liu, Shuying Huang, Weiguo Wan, Wenyong Wen, and Juwei Guan. Infrared and visible image fusion via texture conditional generative adversarial network. *IEEE Transactions on Circuits and Systems for Video Technology*, 31(12):4771–4783, 2021. 2
- [40] Xunpeng Yi, Han Xu, Hao Zhang, Linfeng Tang, and Jiayi Ma. Text-if: Leveraging semantic text guidance for degradation-aware and interactive image fusion. In *Proceedings of the IEEE/CVF Conference on Computer Vision and Pattern Recognition (CVPR)*, pages 27026–27035, 2024. 2, 3, 5
- [41] Meng Yu, Te Cui, Haoyang Lu, and Yufeng Yue. Vifnet: An end-to-end visible-infrared fusion network for image dehazing. *Neurocomputing*, page 128105, 2024. 3
- [42] Jun Yue, Leyuan Fang, Shaobo Xia, Yue Deng, and Jiayi Ma. Dif-fusion: Toward high color fidelity in infrared and visible image fusion with diffusion models. *IEEE Transactions on Image Processing*, 32:5705–5720, 2023. 5
- [43] Syed Waqas Zamir, Aditya Arora, Salman Khan, Munawar Hayat, Fahad Shahbaz Khan, and Ming-Hsuan Yang. Restormer: Efficient transformer for high-resolution image restoration. In *2022 IEEE/CVF Conference on Computer Vision and Pattern Recognition (CVPR)*, pages 5718–5729, 2022. 3, 5
- [44] Hao Zhang, Xuhui Zuo, Jie Jiang, Chunchao Guo, and Jiayi Ma. Mrfs: Mutually reinforcing image fusion and segmentation. In *Proceedings of the IEEE/CVF Conference on Computer Vision and Pattern Recognition (CVPR)*, pages 26974–26983, 2024. 5
- [45] Yafei Zhang, Shen Zhou, and Huafeng Li. Depth information assisted collaborative mutual promotion network for single image dehazing. In *Proceedings of the IEEE/CVF Conference on Computer Vision and Pattern Recognition (CVPR)*, pages 2846–2855, 2024. 5
- [46] Wenda Zhao, Shigeng Xie, Fan Zhao, You He, and Huchuan Lu. Metafusion: Infrared and visible image fusion via meta-feature embedding from object detection. In *Proceedings of the IEEE/CVF Conference on Computer Vision and Pattern Recognition (CVPR)*, pages 13955–13965, 2023. 2
- [47] Huabing Zhou, Wei Wu, Yanduo Zhang, Jiayi Ma, and Haibin Ling. Semantic-supervised infrared and visible image fusion via a dual-discriminator generative adversarial network. *IEEE Transactions on Multimedia*, 25:635–648, 2023. 2